
Beyond Chamfer Distance: Granular Order-aware Evaluation Metric For Online Mapping

Chouaib Bencheikh Lehocine¹ Adam Lilja^{1,2} Junsheng Fu¹ Lars Hammarstrand²
¹Zenseact AB ²Chalmers University of Technology
Gothenburg, Sweden
{firstname.lastname}@{zenseact.com, chalmers.se}

Abstract

Online map estimation is a crucial component of autonomous driving systems that reduces the reliance on costly high-definition maps. State-of-the-art (SOTA) methods commonly predict map elements as ordered sequences of points that form polylines and polygons. The evaluation of these methods relies predominantly on mean average precision (mAP) based on thresholded Chamfer distance (CD). This framework lacks sensitivity to point ordering and provides limited granularity in assessing geometric quality, making it difficult to distinguish which methods truly excel over others. In this work, we address these limitations on two fronts. For the *single-instance similarity measure*, we introduce sequence optimal sub-pattern assignment (SOSPA), an order-aware *metric* that enables fine-grained evaluation of individual geometries while satisfying all metric axioms. For the *multi-instance evaluation framework*, we propose polyline localisation and detection (PLD), a soft *metric* that jointly captures detection quality and geometric accuracy, replacing the hard thresholding of mAP with a principled soft assignment. Through evaluations on nuScenes, we demonstrate that PLD effectively ranks SOTA online mapping methods (MapTRv2, StreamMapNet, MapTracker) while providing a decomposed error analysis. This analysis identifies detection capability as the dominant bottleneck in current methods, revealing a performance trend that mAP fails to capture. Code for evaluation using our metrics will be released.

1 Introduction

Autonomous vehicles require accurate and up-to-date information about the surrounding road geometry to plan safe trajectories. Online map estimation (OME) methods aim to eliminate the reliance on costly pre-built high-definition (HD) maps by predicting map elements using on-board sensors in real time. The performance of downstream planning and control modules is, in turn, directly dependent on these maps. Therefore, the evaluation metrics of OME methods must reflect detection capability as well as geometric accuracy. State-of-the-art (SOTA) OME methods [1, 2, 3, 4, 5, 6] represent map elements such as lane dividers, road boundaries, and pedestrian crossings, as ordered sequences of points forming polylines and polygons, each associated with a confidence score and a semantic class label. Their evaluation rests on two pillars: (i) a *similarity measure* between individual predicted and ground truth geometries, and (ii) a *multi-instance framework* that aggregates element-wise similarities into an overall score. The prevailing evaluation approach employs Chamfer distance (CD) for (i) and average precision (AP) for (ii), with mean average precision (mAP) representing the mean score across predicted classes [1, 2, 3, 4, 5, 6]. This CD-AP combination has two fundamental shortcomings.

First, CD operates on unordered point sets, making it ill-suited as a similarity measure for polylines where point ordering encodes geometric structure. Beyond this, CD measures the joint proximity of full instances, resulting in coarse matching granularity and increased susceptibility to outliers.

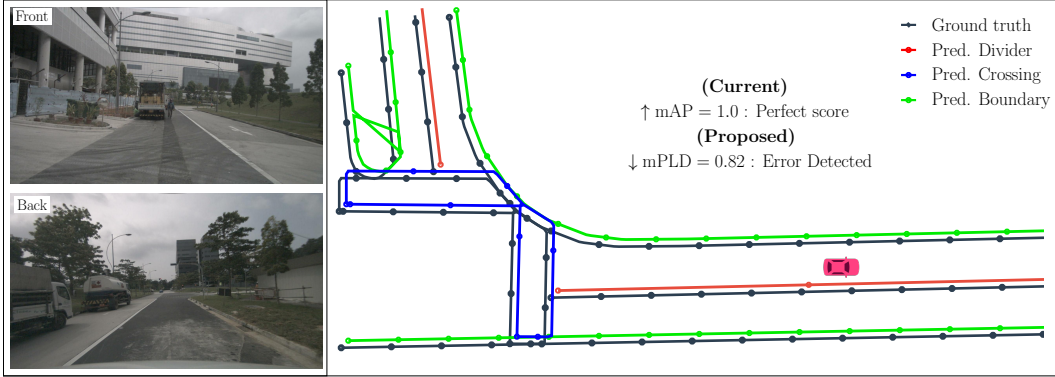


Figure 1: CD-based mAP reports a perfect score of 1.0 for predictions diagonally shifted by 1.0m from the ground truth, with misordering in one instance. Our proposed mPLD correctly penalizes such predictions, yielding a score that reflects the geometric degradation. ($\tau \in \{1.0, 1.5, 2.0\}$ is used for AP, and $c = 1.5, p = 1$ for PLD.)

Additionally, it violates the triangle inequality, rendering it non-metric. The metric axioms (non-negativity, identity, symmetry, and triangle inequality) ensure that an evaluation measure behaves consistently and intuitively, preventing unexpected outcomes such as two identical geometries being rated as dissimilar, or an indirect comparison path yielding a lower cost than a direct one. Some of the limitations of CD can be mitigated by adopting Fréchet distance (FD), as was done in [2, 7], which is order-aware and constitutes a proper metric. However, as a supremum-based measure, FD reflects only the worst-case pointwise error and is therefore sensitive to outliers and uninformative for the remaining geometry (as shown in Section 5.2).

Second, AP converts the similarity measure into hard true positive (TP)/false positive (FP) decisions by thresholding at a set of distance values (e.g., $\{0.5, 1.0, 1.5\}$ m), which discards positional accuracy. Thus, two predictions classified as TPs at the same threshold contribute equally regardless of their geometric accuracy. Furthermore, the thresholds commonly used are permissive relative to the requirements of downstream autonomous driving applications. For instance, even the tightest threshold of 0.5 m implies that a prediction that is 0.5 m offset can still receive a perfect AP score, even though such geometric inaccuracy would critically impact planning and control. An adequate OME evaluation framework should therefore jointly measure detection and geometric accuracy. Furthermore, AP itself does not satisfy the metric axioms, making it a non-principled comparison framework.

To address these shortcomings of existing OME *similarity measures* and *multi-instance framework*, we draw inspiration from the generalized optimal sub-pattern assignment (GOSPA) family of metrics from the multi-object tracking (MOT) literature [8, 9, 10], together with the string matching metric generalized edit distance (GED) [11, 12]. For the *similarity measure*, we introduce sequence optimal sub-pattern assignment (SOSPA), an order-aware adaptation of GOSPA [9] from unordered point sets to sequences of points. GOSPA is an assignment-based metric that optimally matches individual points between two sets and penalizes unmatched points with a tunable cutoff cost c . This cutoff prevents the metric from being dominated by outliers and admits a direct physical interpretation (e.g., maximum tolerable lateral offset). SOSPA inherits these properties while additionally enforcing that matched pairs respect the sequential ordering of points, a key structural property of polylines that GOSPA and CD both ignore. Additionally, we show that the assignment in SOSPA can be cast as a GED minimum-cost assignment problem, enabling its efficient computation via the Wagner–Fischer (WF) algorithm [11] and, provide a bounded normalization in $[0, 1]$ that preserves the metric property. Furthermore, to accommodate comparison between different geometries, we extend SOSPA to polygons (closed polylines) and establish a mathematical result enabling its efficient computation via the cyclic GED algorithm of Maes [12].

For the *multi-instance framework*, we propose PLD, derived from probabilistic-GOSPA (P-GOSPA) [10]. P-GOSPA extends GOSPA to sets of objects with associated existence probabilities, performing soft matching that retains geometric distances in the final score. Since online mapping methods output predicted polylines with confidence scores, this formulation naturally applies. PLD

instantiates P-GOSPA with SOSPA as the base metric, replacing the hard TP/FP classification of AP with a soft assignment that jointly accounts for the SOSPA distance between matched elements and their confidence scores. PLD decomposes into interpretable localization (accuracy) and detection error components, and constitutes a metric. An illustrative comparison between our proposed metric and CD-AP is shown in Fig. 1, where the mean of PLD across map element classes, mPLD, correctly reflects degraded prediction quality, when mAP yields a perfect score.

Our contributions can be summarized as follows. We

- introduce SOSPA, an order-aware polyline metric that satisfies all metric axioms, providing finer granularity in detecting matches and mismatches, while being robust to outliers,
- show that SOSPA is equivalent to a GED minimum-cost trace problem allowing its efficient computation, and derive a normalized form bounded in $[0, 1]$ that remains a metric for $p = 1$,
- define cyclic SOSPA for polygons and establish a lemma enabling its efficient computation,
- propose PLD, a soft multi-instance metric jointly quantifying detection and positional accuracy with an inherent decomposition into localization and detection errors, and
- benchmark SOTA online mapping methods on nuScenes [13], showing that PLD preserves relative performance rankings indicated by AP while its error decomposition reveals that detection error dominates across all methods, a finding that AP can not capture.

2 Related work

Online vectorized mapping. OME alleviates reliance on HD maps in autonomous driving. Following the shift from rasterized to vectorized output initiated by HDMaPNet [1], a range of DETR-inspired architectures [14] have been proposed for vectorized end-to-end map construction, including VectorMapNet [2], MapTR [3], and MapTRv2 [4]. Temporal fusion has been recently incorporated in methods such as StreamMapNet [5] and MapTracker [6] to further improve consistency and extend detection range. Despite these architectural advancements, evaluation practices, predominantly AP with CD, have not kept pace, limiting our ability to fully assess progress in this area.

GOSPA-family MOT metrics. Optimal sub-pattern assignment (OSPA) [8] introduced a proper metric for MOT evaluation over finite sets. GOSPA [9] generalized it by removing normalization and allowing flexible penalization of missed and false detections, with subsequent extensions to trajectories [15], graphs [16], and random finite sets (RFSs) in P-GOSPA [10]. In particular, P-GOSPA incorporates existence probabilities and covariances from multi-Bernoulli (MB) RFS, enabling probabilistic soft detection decisions for matches and mismatches. All these GOSPA-family metrics share a key merit, which is their decomposition into interpretable error terms associated with matched and unmatched instances. We leverage this property in PLD, which is built on P-GOSPA with SOSPA as its underlying single-instance matching metric. SOSPA extends GOSPA from unordered sets to ordered sequences and reintroduces normalization to support OME instance matching.

Generalized edit distance. Comparing ordered sequences has a long history in string matching applications, such as text retrieval and computational biology [17]. GED (also known as Levenshtein distance) [18, 11, 12, 17] is a metric that quantifies the cost of transforming one string (i.e., sequence) into another through substitution, insertion, and deletion operations. Normalization into bounded metrics has been studied in [19, 17], while cyclic variants for closed structures were introduced in [12]. GED is computed in $\mathcal{O}(|x| \cdot |y|)$ time via dynamic programming using the WF algorithm [11], which solves a minimum-cost trace problem. Our SOSPA formulation can be cast as a minimum-cost trace problem, enabling efficient computation using existing GED algorithms.

3 Order-aware polyline similarity metric: SOSPA

To improve the evaluation of OME methods, we address the limitations of existing similarity measures by introducing SOSPA, an order-aware similarity metric for finite point sequences, i.e., polylines. We treat open polylines (Section 3.1) and polygons (Section 3.2) separately and address normalization and computation.

3.1 Sequence optimal sub-pattern assignment

We begin by defining $\mathbf{x} = (x_1, \dots, x_{|\mathbf{x}|})$ and $\mathbf{y} = (y_1, \dots, y_{|\mathbf{y}|})$ to be finite sequences of points in \mathbb{R}^N . An assignment set between \mathbf{x} and \mathbf{y} is any subset $\theta \subseteq \{1, \dots, |\mathbf{x}|\} \times \{1, \dots, |\mathbf{y}|\}$ satisfying the uniqueness constraint that each index appears at most once. The collection of all valid assignment sets between \mathbf{x} and \mathbf{y} is denoted by $\Gamma_{|\mathbf{x}|, |\mathbf{y}|}$. An assignment set $\theta = \{(i_k, j_k)\}_{k=1}^{|\theta|} \in \Gamma_{|\mathbf{x}|, |\mathbf{y}|}$ is said to be an *ordered* assignment set if its index pairs respect a strictly increasing order. That is, $i_1 < i_2 < \dots < i_{|\theta|}$, and $j_1 < j_2 < \dots < j_{|\theta|}$. The set of all ordered assignment sets between \mathbf{x} and \mathbf{y} is denoted by $\Gamma_{|\mathbf{x}|, |\mathbf{y}|}^o$.

Definition 1. Given a metric $d(\cdot, \cdot)$ in \mathbb{R}^N , a scalar $c > 0$, and a scalar p where $1 \leq p < \infty$,

$$d_{SOSPA}^{(c,p)}(\mathbf{x}, \mathbf{y}) = \left(\min_{\theta \in \Gamma_{|\mathbf{x}|, |\mathbf{y}|}^o} \sum_{(i,j) \in \theta} d(x_i, y_j)^p + \frac{c^p}{2} (|\mathbf{x}| + |\mathbf{y}| - 2|\theta|) \right)^{1/p}. \quad (1)$$

From the definition, it follows immediately that SOSPA satisfies identity, non-negativity, and symmetry. The proof for the triangle inequality can be found in Appendix B.

The main difference between SOSPA and GOSPA [9] with $(\alpha = 2)$ is that SOSPA is defined over sequences instead of sets, thus constraining the matches to be ordered (i.e., $\theta \in \Gamma^o$). The cutoff distance c in (1) defines the maximum allowable error for pairs to be regarded as matched points, as well as the penalty for missed and false detections given by $c^p/2$. The exponent $p \geq 1$ determines the sensitivity of the metric to localization errors, where a higher p results in higher penalization of large deviations among matched pairs. The use of a constant penalty $c^p/2$ per unmatched point ensures the robustness of the metric to outliers, since they cannot excessively influence the final score. Furthermore, while the overall matching must respect the sequential order of points in both sequences, the formulation allows individual points in each sequence to be skipped (i.e., left unmatched) for $c^p/2$ per skipped point, providing flexibility in handling sequences of unequal length, or locally poor correspondence.

Computing SOSPA. The ordering constraint in (1) makes the underlying optimization problem for SOSPA fundamentally different from the bipartite matching problem in GOSPA, which can be efficiently solved using the Hungarian algorithm. To find an efficient solution to (1), we propose to cast it as a minimum-cost trace problem from the GED literature [11, 19]. GED measures the minimum cost of transforming a sequence \mathbf{x} into \mathbf{y} through (i) substitutions $x_i \rightarrow y_j$ at cost $\gamma(x_i \rightarrow y_j) \geq 0$, (ii) deletions $x_i \rightarrow \Lambda$ at cost $\gamma(x_i \rightarrow \Lambda) \geq 0$, and (iii) insertions $\Lambda \rightarrow y_j$ at cost $\gamma(\Lambda \rightarrow y_j) \geq 0$, where Λ is the null element. A *trace* is a set T of index pairs that respects sequence ordering, i.e., an ordered assignment set. Its cost is

$$C(T) = \sum_{(i,j) \in T} \gamma(x_i \rightarrow y_j) + \sum_{i \notin \pi_1(T)} \gamma(x_i \rightarrow \Lambda) + \sum_{j \notin \pi_2(T)} \gamma(\Lambda \rightarrow y_j), \quad (2)$$

where $\pi_1(T) = \{i : (i, j) \in T\}$ and $\pi_2(T) = \{j : (i, j) \in T\}$ are index projections of T . We now show that SOSPA is equivalent to a minimum cost trace of GED with specific cost functions.

Lemma 1. $d_{SOSPA}^{(c,p)}(\mathbf{x}, \mathbf{y})^p$ equals the minimum trace cost of GED between \mathbf{x} and \mathbf{y} with cost functions

$$\gamma(x_i \rightarrow y_j) = d(x_i, y_j)^p, \quad \gamma(x_i \rightarrow \Lambda) = \gamma(\Lambda \rightarrow y_j) = \frac{c^p}{2}. \quad (3)$$

Proof. Substituting (3) into (2) and noting that traces are ordered assignment sets, the minimum trace cost, $\min_T C(T)$, coincides with (1) raised to the power p . \square

By Lemma 1, SOSPA can be computed via dynamic programming (DP) using the WF algorithm [11] (equivalently, Needleman-Wunsch algorithm [20]) in $\mathcal{O}(|\mathbf{x}| \cdot |\mathbf{y}|)$ time.

Remark 1. When $\gamma(\cdot \rightarrow \cdot)$ is a metric, GED coincides with the minimum trace cost $\min_T C(T)$ [11] and is a metric. The costs in (3) satisfy these conditions for $p = 1$ (since $d(\cdot, \cdot)^p$ is a metric when $p = 1$), providing an alternative proof of the triangle inequality for SOSPA (see Appendix for the direct proof covering all $p \geq 1$). Given $\gamma(\cdot \rightarrow \cdot)$ is not a metric, the minimum-cost trace problem remains well-defined for any non-negative cost function, and the WF algorithm solves it regardless. Hence, the WF algorithm correctly computes SOSPA for all $p \geq 1$.

Normalization of SOSPA. To facilitate the use of SOSPA as a polyline matching metric, we normalize $d_{\text{SOSPA}}^{(c,p)}$ while preserving its metric property. A natural normalization is $d_{\text{SOSPA}}^{(c,p)} / (\frac{c^p}{2}(|\mathbf{x}| + |\mathbf{y}|))^{1/p}$. However, this does not satisfy the triangle inequality in general. Instead, following the approach used to normalize GED in [17], we define $\bar{d}_{\text{SOSPA}}^{(c,p)}$ as follows.

Definition 2. Let $d_{\text{SOSPA}}^{(c,p)}$ be as defined in (1). Then

$$\bar{d}_{\text{SOSPA}}^{(c,p)}(\mathbf{x}, \mathbf{y}) = \frac{2 \cdot d_{\text{SOSPA}}^{(c,p)}(\mathbf{x}, \mathbf{y})}{(\frac{c^p}{2}(|\mathbf{x}| + |\mathbf{y}|))^{1/p} + d_{\text{SOSPA}}^{(c,p)}(\mathbf{x}, \mathbf{y})} \in [0, 1]. \quad (4)$$

For $p = 1$, $\bar{d}_{\text{SOSPA}}^{(c,p)}$ satisfies the triangle inequality as shown in Appendix B.2, and is thus a metric (identity and symmetry follow from $d_{\text{SOSPA}}^{(c,p)}$).

3.2 SOSPA for polygons

Since the starting point of a polygon (i.e., closed polyline) can be changed without altering its geometry, computing SOSPA for polygons (i.e., closed polylines) requires inspecting all cyclic shift combinations of the polygons. The same difficulty arises for cyclic FD [21] and cyclic GED [12]. Therefore, in the following, we define SOSPA over cyclic sequences and establish a Lemma that enables solving it using an efficient exact algorithm that leverages cyclic shift properties.

Let $\langle k \rangle_n$ denote a cyclic shift operation following

$$\langle k \rangle_n = ((k - 1) \bmod n) + 1, \quad k \in \mathbb{Z}, n \in \mathbb{N}^+. \quad (5)$$

Then, define the cyclically shifted version of the sequence \mathbf{x} as

$$\mathcal{S}_s(\mathbf{x}) = (x_{\langle 1+s \rangle_{|\mathbf{x}|}}, x_{\langle 2+s \rangle_{|\mathbf{x}|}}, \dots, x_{\langle |\mathbf{x}|+s \rangle_{|\mathbf{x}|}}), \quad s \in \mathbb{Z}. \quad (6)$$

We can now readily denote the set of all cyclic shifts of a finite sequence as $[\mathbf{x}] = \{\mathcal{S}_l(\mathbf{x}) : 0 \leq l \leq |\mathbf{x}| - 1\}$, and this will be referred to as a cyclic sequence.

Definition 3. Given that two finite cyclic sequences $[\mathbf{x}]$ and $[\mathbf{y}]$, then SOSPA is defined as

$$d_{\text{SOSPA}}^{(c,p)}([\mathbf{x}], [\mathbf{y}]) = \min_{\substack{s_x \in \{0, \dots, |\mathbf{x}|-1\} \\ s_y \in \{0, \dots, |\mathbf{y}|-1\}}} d_{\text{SOSPA}}^{(c,p)}(\mathcal{S}_{s_x}(\mathbf{x}), \mathcal{S}_{s_y}(\mathbf{y})). \quad (7)$$

A straightforward evaluation of (7) requires $|\mathbf{x}||\mathbf{y}|$ computations of SOSPA. Following a key result for cyclic GED [12, Lemma 3.1], we show that optimizing over the cyclic shifts of one sequence while fixing the other suffices.

Lemma 2. For any two finite cyclic sequences $[\mathbf{x}]$ and $[\mathbf{y}]$, we have

$$d_{\text{SOSPA}}^{(c,p)}([\mathbf{x}], [\mathbf{y}]) = d_{\text{SOSPA}}^{(c,p)}(\mathbf{x}, [\mathbf{y}]) = \min_{s_y \in \{0, \dots, |\mathbf{y}|-1\}} d_{\text{SOSPA}}^{(c,p)}(\mathbf{x}, \mathcal{S}_{s_y}(\mathbf{y})). \quad (8)$$

Proof. The proof follows a similar argument to one outlined in [12, Lemma 3.1]. See Appendix D for details. \square

Using the result above, and the established relation between GED and SOSPA in Lemma 1, the cyclic SOSPA can be computed efficiently using Maes algorithm [12] in $\mathcal{O}(|\mathbf{x}||\mathbf{y}| \log |\mathbf{y}|)$ time, and faster cyclic GED algorithms such as [22] directly apply. We note that the original reference on cyclic GED [12] does not establish whether cyclic GED constitutes a metric (the same is true for cyclic FD [21]). As cyclic SOSPA shares a similar structural formulation with cyclic GED, we likewise do not claim it to be a metric, as we believe it does not satisfy the triangle inequality in general.

4 Multi-instance evaluation metric: PLD

To score OME methods, we need a multi-instance evaluation measure. While SOSPA can be combined with AP, this combination still inherits AP rigid matching strategy and discards the geometric accuracy. Therefore, in this section, we introduce PLD, a soft multi-instance metric that jointly evaluates detection and geometric accuracy.

4.1 Online mapping outputs as multi-Bernoulli RFS

For each road element class, an OME method outputs $\mathbf{X} = \{(r_i, \mathbf{x}_i)\}_{i=1}^{|\mathbf{X}|}$, where $r_i \in [0, 1]$ is the confidence score of the i -th instance and \mathbf{x}_i is a polyline (i.e., a finite sequence of points in \mathbb{R}^N) describing its estimated geometry. The output \mathbf{X} parametrizes a MB RFS distribution over sequences, where each component (r_i, \mathbf{x}_i) constitutes an independent Bernoulli process with existence probability r_i and a degenerate single-object density concentrated at the polyline \mathbf{x}_i . Ground truth instances take the same form with $r_i = 1$ for all i . This probabilistic interpretation of OME outputs promotes the use of P-GOSPA [10], a metric designed for comparing MB distributions, as a multi-instance evaluation framework. Accordingly, we define PLD as the instantiation of P-GOSPA that uses $\bar{d}_{\text{SOSPA}}^{(c,p)}$ as the base single-instance distance, and adopt it as our multi-instance evaluation metric.

4.2 Polyline localisation and detection error metric

Definition 4. For sets of polylines \mathbf{X} and \mathbf{Y} , $c > 0$ and $1 \leq p < \infty$,

$$d_{\text{PLD}}^{(c,p)}(\mathbf{X}, \mathbf{Y}) = \left[\min_{\theta \in \Gamma} \left(\sum_{(i,j) \in \theta} \left[\min(r_{\mathbf{x}_i}, r_{\mathbf{y}_j}) \bar{d}_{\text{SOSPA}}^{(c,p)}(\mathbf{x}_i, \mathbf{y}_j)^p + \frac{1}{2} |r_{\mathbf{x}_i} - r_{\mathbf{y}_j}| \right] + \frac{1}{2} \left(\sum_{i: \forall j, (i,j) \notin \theta} r_{\mathbf{x}_i} + \sum_{j: \forall i, (i,j) \notin \theta} r_{\mathbf{y}_j} \right) \right) \right]^{\frac{1}{p}}. \quad (9)$$

where $\bar{d}_{\text{SOSPA}}^{(c,p)}$ is defined in (4), and where $\theta \in \Gamma$ is an assignment set between \mathbf{X} and \mathbf{Y} .

This is P-GOSPA [10, Proposition. 2] with $\alpha = 2$, $c = 1$, and $\bar{d}_{\text{SOSPA}}^{(c,p)}$ as the base distance. Since $\bar{d}_{\text{SOSPA}}^{(c,p)}$ is a metric for $p = 1$, so is PLD by [10, Proposition. 2]. The minimization is a 2D assignment problem, solvable in polynomial time by the Hungarian algorithm.

Looking at (9), the role of confidence scores becomes clear. Unmatched instances incur a penalty proportional to their confidence. A high-confidence miss or false alarm is penalized more than an uncertain one, reflecting the intuition that confident errors are more consequential. For matched pairs, the cost combines a confidence-weighted geometric term with a confidence-mismatch term $\frac{1}{2}|r_{\mathbf{x}_i} - r_{\mathbf{y}_j}|$, which penalizes disagreement between predicted and ground truth existence probabilities. Consequently, a good match requires not only geometric accuracy but also well-calibrated confidence. This makes PLD a comprehensive measure for evaluating probabilistic map instances as produced by online mapping methods. Although ground-truth carries $r_j = 1$, (9) is fully general and supports comparing two stochastic outputs (e.g. for measuring temporal consistency between consecutive map predictions).

PLD decomposition into interpretable error terms. Letting θ^* denote the optimal assignment in (9), define

$$e_{\text{loc.}}^{(c,p)}(\mathbf{X}, \mathbf{Y}) = \sum_{(i,j) \in \theta^*} \min(r_{\mathbf{x}_i}, r_{\mathbf{y}_j}) \bar{d}_{\text{SOSPA}}^{(c,p)}(\mathbf{x}_i, \mathbf{y}_j)^p, \quad (10)$$

$$e_{\text{det.}}(\mathbf{X}, \mathbf{Y}) = \sum_{(i,j) \in \theta^*} \frac{1}{2} |r_{\mathbf{x}_i} - r_{\mathbf{y}_j}| + \frac{1}{2} \left(\sum_{i: (i,j) \notin \theta^*} r_{\mathbf{x}_i} + \sum_{j: (i,j) \notin \theta^*} r_{\mathbf{y}_j} \right), \quad (11)$$

so that $d_{\text{PLD}}^{(c,p)}(\mathbf{X}, \mathbf{Y}) = [e_{\text{loc.}}^{(c,p)}(\mathbf{X}, \mathbf{Y}) + e_{\text{det.}}(\mathbf{X}, \mathbf{Y})]^{1/p}$. The term $e_{\text{loc.}}^{(c,p)}$ is a probability-weighted aggregation of geometric error over matched pairs. The quantity $e_{\text{det.}}$ pools detection-related penalties: confidence mismatch on matched pairs, missed instances, and false alarms. Including confidence mismatch within the detection term is justified by the fact that a matched instance with confidence r behaves as a $(1 - r)$ -weighted false detection. The constant $\frac{1}{2}$ on detection penalties keeps the metric robust to outliers.

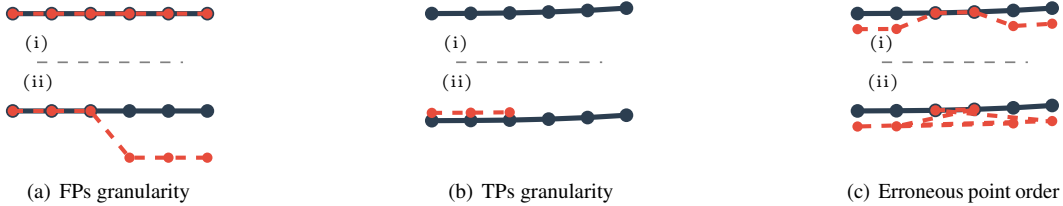


Figure 2: Illustrative examples highlighting the advantages of PLD. All confidences set to 1.

Table 1: PLD ($c = 0.5, p = 1$) versus CD/FD-AP ($\tau = 0.5$) on the illustrative examples in Fig. 2

Case	PLD			CD-AP	FD-AP	
	val.	Loc.	Det.	val.	val.	
FPs granularity (Fig. 2(a))	(i)	0.0	0.0	0.0	1.0	1.0
	(ii)	0.800	0.0	0.800	1.0	0.0
TPs granularity (Fig. 2(b))	(i)	1.000	0.0	1.000	0.0	0.0
	(ii)	0.778	0.222	0.556	0.0	0.0
Erroneous Order (Fig. 2(c))	(i)	0.593	0.593	0.0	1.0	1.0
	(ii)	0.778	0.222	0.556	1.0	0.0

Normalization of PLD. To facilitate comparability across categories and baselines, we apply the same normalization as used for SOSPA. That is,

$$\bar{d}_{\text{PLD}}^{(c,p)}(\mathbf{X}, \mathbf{Y}) = \frac{2 d_{\text{PLD}}^{(c,p)}(\mathbf{X}, \mathbf{Y})}{\left(\frac{1}{2}(R_{\mathbf{X}} + R_{\mathbf{Y}})\right)^{1/p} + d_{\text{PLD}}^{(c,p)}(\mathbf{X}, \mathbf{Y})} \in [0, 1], \quad (12)$$

where $R_{\mathbf{X}} = \sum_i r_{\mathbf{x}_i}$ and $R_{\mathbf{Y}} = \sum_j r_{\mathbf{y}_j}$. The normalized PLD is positive and symmetric. Moreover, for the case $p = 1$, it does satisfy the triangle inequality as shown in Appendix B.2 and is therefore a metric. Beyond satisfying the triangle inequality, the case $p = 1$ enables a particularly convenient use of the decomposition terms. Specifically, (9) simplifies to $d_{\text{PLD}}^{(c,1)} = e_{\text{loc.}}^{(c,1)} + e_{\text{det.}}$, and the decomposition extends naturally to the normalized form with

$$\bar{e}_{\text{loc.}}^{(c,1)}(\mathbf{X}, \mathbf{Y}) = \frac{2 e_{\text{loc.}}^{(c,1)}(\mathbf{X}, \mathbf{Y})}{\frac{1}{2}(R_{\mathbf{X}} + R_{\mathbf{Y}}) + d_{\text{PLD}}^{(c,1)}(\mathbf{X}, \mathbf{Y})}, \quad \bar{e}_{\text{det.}}(\mathbf{X}, \mathbf{Y}) = \frac{2 e_{\text{det.}}(\mathbf{X}, \mathbf{Y})}{\frac{1}{2}(R_{\mathbf{X}} + R_{\mathbf{Y}}) + d_{\text{PLD}}^{(c,1)}(\mathbf{X}, \mathbf{Y})}, \quad (13)$$

giving $\bar{d}_{\text{PLD}}^{(c,1)} = \bar{e}_{\text{loc.}}^{(c,1)} + \bar{e}_{\text{det.}}$. We use $p = 1$ throughout the experiments.

5 Experiments

In this section, we highlight the advantages of PLD and SOSPA using illustrative examples. We then benchmark three SOTA OME methods on nuScenes [13], the most widely adopted benchmark for OME.

5.1 Results from illustrative examples

Fig. 2 shows three scenarios specifically constructed to highlight limitations of CD/FD-AP, with results reported in Table 1. For Fig. 2(a), CD-AP returns a perfect score for *both* predictions, even though prediction (ii) includes spurious points. PLD correctly assigns prediction (ii) a higher error, attributed entirely to $\bar{e}_{\text{det.}}$ (Det.). FD-AP also detects the false positive points, but due to its supremum-based formulation, it excessively penalizes the prediction, resulting in $\text{AP} = 0$. For Fig. 2(b), CD-AP fails to distinguish between a partial match and no match at all, both yielding $\text{AP} = 0$, as does FD-AP. In contrast, PLD ranks the partial match higher and, through its error decomposition, captures both the partial matching and the associated accuracy error. For Fig. 2(c), prediction (ii) has the same

Table 2: AP results for different baselines based on both CD and FD.

Baseline	↑ CD-AP				↑ FD-AP				
	Crossing	Divider	Boundary	mAP ¹	Crossing	Divider	Boundary	mAP	
R ₆₀	MapTRv2	0.127	0.262	0.445	0.278	0.052	0.107	0.292	0.150
	StreamMapNet	0.316	0.283	0.407	0.335	0.150	0.132	0.257	0.180
	MapTracker	0.441	0.288	0.440	0.390	0.242	0.130	0.295	0.222
R ₁₀₀	MapTRv2	0.081	0.174	0.293	0.183	0.017	0.020	0.051	0.029
	StreamMapNet	0.249	0.167	0.241	0.219	0.036	0.020	0.036	0.031
	MapTracker	0.455	0.235	0.381	0.357	0.147	0.040	0.085	0.091

Table 3: PLD results for different baselines with $c = 1.5$, $p = 1$.

Baseline	Crossing	Divider	Boundary	↓ mPLD	mLoc.	mDet.	
R ₆₀	Maptrv2	0.943	0.899	0.837	0.893	0.184	0.709
	StreamMapNet	0.895	0.870	0.832	0.866	0.249	0.617
	MapTracker	0.832	0.849	0.785	0.822	0.276	0.546
R ₁₀₀	Maptrv2	0.966	0.939	0.903	0.936	0.144	0.792
	StreamMapNet	0.939	0.932	0.914	0.928	0.188	0.740
	MapTracker	0.883	0.904	0.864	0.884	0.227	0.657

point positions as prediction (i), but with a scrambled order. CD-AP reports 1.0 in both cases. FD-AP correctly detects the misordering, but penalizes it heavily yielding AP = 0. PLD not only detects the misordering but also penalizes it appropriately, assigning PLD < 1.0. The decomposition is particularly insightful in this case, as $\bar{e}_{\text{det.}} = 0$ for the correct ordering and $\bar{e}_{\text{det.}} > 0$ for the scrambled one. These observations confirm that, by construction, PLD provides finer granularity in identifying TPs and FPs, and is sensitive to misordering, both merits inherited from its SOSPA base.

5.2 Benchmark OME methods on nuScenes

Setup. We evaluate three SOTA methods MapTRv2 [4], StreamMapNet [5], and MapTracker [6], on the new nuScenes split of [5] that addresses geographic data leakage issue (also reported in [23]). We retrain MapTRv2 on this split. Predictions and ground truth are equidistantly sampled at 0.5 m (see discussion in Appendix A.1). We report results at two evaluation ranges, corresponding to a near-field range R₆₀ = 60 × 30 m and a long range R₁₀₀ = 100 × 50 m. We evaluate AP and PLD for pedestrian crossing, divider, and boundary. The average performance across classes is reported using mAP and mPLD, respectively. The standard thresholds $\tau \in \{0.5, 1.0, 1.5\}$ m for R₆₀ and $\{1.0, 1.5, 2.0\}$ m for R₁₀₀ are used for CD-AP. We additionally evaluate FD-AP using the thresholds $\tau \in \{1.0, 2.0, 3.0\}$ m from OpenLaneV2 [7]. Since these thresholds are already extensive, we apply them for both R₆₀ and R₁₀₀. For PLD, since the metric already accounts for both detection and accuracy in a single score, we use a *single* cutoff $c = 1.5$ for both ranges (additional values are tested in Section A.2). When evaluating PLD, we compute SOSPA using (1) for polylines and (7) for polygons (with duplicate closing points removed), with $p = 1$ in both cases. To handle directionality, we evaluate SOSPA for each instance pair under the original ordering and with one instance direction reversed, selecting the minimum value.

Comparing methods. Table 2 reports AP and Table 3 reports PLD and its decomposition. Looking at FD-AP results, we see that despite the extensive thresholds used, the scores on R₁₀₀ are near zero for all methods (e.g., mAP of 0.029, 0.031, and 0.091), rendering them uninformative to a practitioner seeking to differentiate method quality at longer range. Comparing CD-based mAP and mPLD, we see that the two frameworks agree on the relative ranking across both ranges. That is, MapTracker outperforms StreamMapNet, which in turn outperforms MapTRv2. This consistency confirms that PLD captures the essential performance differences. Beyond this agreement, the PLD decomposition reveals a structural pattern that mAP cannot expose. That is, across all methods and both ranges,

¹Differences with [5, 6] are due to fixed- N point sampling (e.g. for R₆₀, StreamMapNet and MapTracker report 0.341 and 0.403).

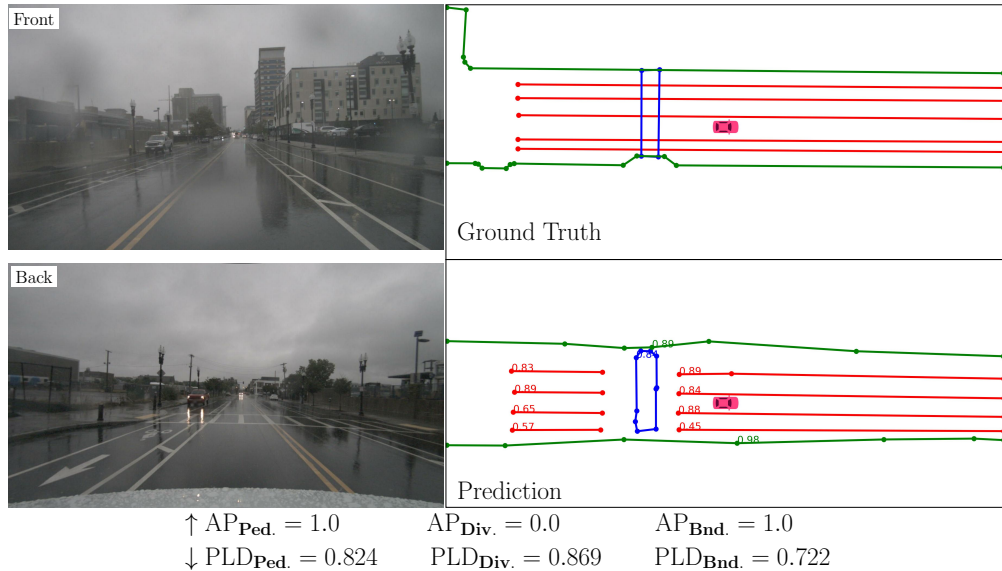


Figure 3: Qualitative example from MapTracker on R_{100} , comparing AP to PLD for pedestrian crossing (blue), divider (red), and boundary (green). ($\tau \in \{1.0, 1.5, 2.0\}$ is used for AP, and $c = 1.5$, $p = 1$ for PLD. Confidences are shown on the figure.)

the detection error $\bar{e}_{\text{det.}}$ (mDet.) dominates the localization error $\bar{e}_{\text{loc.}}^{(c,p)}$ (mLoc.) by a factor of two to four. Detection capability, i.e., missed instances and false alarms, is currently the primary bottleneck for OME, not geometric precision per detected element. The gap widens at the longer R_{100} range, indicating that detection coverage is harder to maintain as range increases.

Qualitative Comparison. Fig. 3 highlights the binary nature of AP across classes. For example, AP assigns a perfect score to the boundary class even though part of the left road edge is missed, while rating dividers as unusable despite predictions falling within an acceptable distance. In contrast, PLD more accurately reflects that boundary detections are imperfect and dividers are not entirely unusable, yielding a more meaningful assessment of prediction quality. PLD could be further improved by allowing multiple-to-multiple instance assignments with penalties for instance fragmentation or merging, as in trajectory-GOSPA [15], and is left for future work. For more qualitative examples, see Appendix A.3.

Runtime. Benchmarking the evaluation time using StreamMapNet on R_{60} , mPLD achieves comparable runtime to CD-based mAP (≈ 38 s each with 64 workers). This shows that PLD advantages do not come at the cost of runtime. For more details, see the analysis in Appendix A.1.

6 Conclusions

To improve the understanding of OME methods, we introduced SOSPA, an order-aware polyline similarity metric, and PLD, a soft multi-instance evaluation metric, as alternatives to CD-based mAP for evaluating OME methods. Both satisfy metric axioms, remain computationally tractable, and jointly capture detection and positional accuracy. Benchmarking three SOTA methods on nuScenes shows that PLD preserves relative performance rankings while its error decomposition reveals that detection error dominates across all methods, a finding that mAP fails to capture.

Limitations and future work. Our framework focuses on geometry, and instance-level topological structure (e.g. which lanes connect to which) is not captured. One promising direction for future work is therefore to investigate topology-aware extensions of SOSPA and PLD [16, 7]. Additionally, while we focus on nuScenes for its popularity, evaluating on additional datasets and on other methods would further test the generality of the framework.

Finally, we hope that an order-aware, decomposable, metric-based evaluation framework will support continued progress in online mapping for safer autonomous driving.

References

- [1] Q. Li, Y. Wang, Y. Wang, and H. Zhao. HDMaPNet: An online HD map construction and evaluation framework. In *Proc. 2022 IEEE Int. Conf. Robot. Autom. (ICRA)*, pages 4628–4634, 2022.
- [2] Y. Liu, T. Yuan, Y. Wang, Y. Wang, and H. Zhao. VectorMapNet: End-to-end vectorized HD map learning. In *Proc. 40th Int. Conf. Mach. Learn. (ICML)*, volume 202 of *Proc. Mach. Learn. Res.*, pages 22352–22369. PMLR, 2023.
- [3] B. Liao, S. Chen, X. Wang, T. Cheng, Q. Zhang, W. Liu, and C. Huang. MapTR: Structured modeling and learning for online vectorized HD map construction. In *Proc. Int. Conf. Learn. Represent. (ICLR)*, 2023.
- [4] B. Liao, S. Chen, Y. Zhang, B. Jiang, Q. Zhang, W. Liu, C. Huang, and X. Wang. MapTRv2: An end-to-end framework for online vectorized HD map construction. *Int. J. Comput. Vis.*, pages 1–23, 2024.
- [5] T. Yuan, Y. Liu, Y. Wang, Y. Wang, and H. Zhao. StreamMapNet: Streaming mapping network for vectorized online HD map construction. In *Proc. IEEE/CVF Winter Conf. Appl. Comput. Vis. (WACV)*. IEEE, 2024.
- [6] J. Chen, Y. Wu, J. Tan, H. Ma, and Y. Furukawa. MapTracker: Tracking with strided memory fusion for consistent vector HD mapping. In *Proc. Eur. Conf. Comput. Vis. (ECCV)*, Lecture Notes in Computer Science. Springer, 2024. Oral presentation.
- [7] H. Wang, T. Li, Y. Li, L. Chen, C. Sima, Z. Liu, B. Wang, P. Jia, Y. Wang, S. Jiang, F. Wen, H. Xu, P. Luo, J. Yan, W. Zhang, and H. Li. Openlane-v2: A topology reasoning benchmark for unified 3d HD mapping. In *Proc. 37th Int. Conf. Neural Inf. Process. Syst. (NeurIPS)*, pages 827–838, New Orleans, LA, USA, 2023. Curran Associates Inc.
- [8] D. Schuhmacher, B.-T. Vo, and B.-N. Vo. A consistent metric for performance evaluation of multi-object filters. *IEEE Trans. Signal Process.*, 56(9):3447–3457, September 2008.
- [9] A. S. Rahmathullah, Á. F. García-Fernández, and L. Svensson. Generalized optimal sub-pattern assignment metric. In *Proc. 20th Int. Conf. Inf. Fusion (Fusion)*. IEEE, July 2017.
- [10] Y. Xia, Á. F. García-Fernández, J. Karlsson, T. Yuan, K.-C. Chang, and L. Svensson. Probabilistic GOSPA: A metric for performance evaluation of multi-object filters with uncertainties. *IEEE Trans. Aerosp. Electron. Syst.*, 2025.
- [11] R. A. Wagner and M. J. Fischer. The string-to-string correction problem. *J. ACM*, 21(1):168–178, 1974.
- [12] M. Maes. On a cyclic string-to-string correction problem. *Inf. Process. Lett.*, 35(2):73–78, 1990.
- [13] H. Caesar, V. Bankiti, A. H. Lang, S. Vora, V. E. Liong, Q. Xu, A. Krishnan, Y. Pan, G. Baldan, and O. Beijbom. nuScenes: A multimodal dataset for autonomous driving. In *Proc. IEEE/CVF Conf. Comput. Vis. Pattern Recognit. (CVPR)*, pages 11621–11631, 2020.
- [14] N. Carion, F. Massa, G. Synnaeve, N. Usunier, A. Kirillov, and S. Zagoruyko. End-to-end object detection with transformers. In *Proc. Eur. Conf. Comput. Vis. (ECCV)*, pages 213–229, Cham, Switzerland, 2020. Springer International Publishing.
- [15] Á. F. García-Fernández, A. S. Rahmathullah, and L. Svensson. A metric on the space of finite sets of trajectories for evaluation of multi-target tracking algorithms. *IEEE Trans. Signal Process.*, 68:3917–3928, 2020.
- [16] J. Gu, Á. F. García-Fernández, R. E. Firth, and L. Svensson. Graph GOSPA metric: A metric to measure the discrepancy between graphs of different sizes. *IEEE Trans. Signal Process.*, 72:4037–4049, 2024.

- [17] Y. Li and B. Liu. A normalized levenshtein distance metric. *IEEE Trans. Pattern Anal. Mach. Intell.*, 29(6):1091–1095, 2007.
- [18] V. I. Levenshtein. Binary codes capable of correcting deletions, insertions, and reversals. *Soviet Physics Doklady*, 10(8):707–710, 1966.
- [19] A. Marzal and E. Vidal. Computation of normalized edit distance and applications. *IEEE Trans. Pattern Anal. Mach. Intell.*, 15(9):926–932, 1993.
- [20] S. B. Needleman and C. D. Wunsch. A general method applicable to the search for similarities in the amino acid sequence of two proteins. *J. Molecular Biology*, 48(3):443–453, 1970.
- [21] E. Vodolazskiy. Discrete Fréchet distance for closed curves. *Comput. Geom.*, 111:101967, 2023.
- [22] A. Marzal and S. Barrachina. Speeding up the computation of the edit distance for cyclic strings. In *Proc. 15th Int. Conf. Pattern Recognit. (ICPR)*, volume 2, pages 891–894, 2000.
- [23] A. Lilja, J. Fu, E. Stenborg, and L. Hammarstrand. Localization is all you evaluate: Data leakage in online mapping datasets and how to fix it. In *Proc. IEEE/CVF Conf. Comput. Vis. Pattern Recognit. (CVPR)*. IEEE, 2024.

Table 4: Effect of sampling distance on mPLD ($c = 1.5, p = 1$) and CD-mAP benchmarked using StreamMapNet on R_{60} . The runtime is based on the average of multiple runs with 64 workers.

Samp. (m)	↑ mAP		↓ mPLD		$\bar{e}_{loc.}^{(c,p)}$		$\bar{e}_{det.}$		mAP mPLD		
	val.	Δ	val.	Δ	val.	Δ	val.	Δ	Runtime (s)		Δ
0.25	0.345	+3.0%	0.860	-0.7%	0.241	-3.2%	0.619	+0.3%	65.9	87.0	+32%
0.50	0.335	—	0.866	—	0.249	—	0.617	—	38.0	37.8	-1%
0.75	0.323	-3.6%	0.873	+0.8%	0.259	+4.0%	0.614	-0.5%	28.5	31.6	+11%
$N = 200$	0.347	+3.6%	0.866	0.0%	0.234	-6.0%	0.632	+2.4%	160.1	238.2	+49%

A Additional experimental results

This section presents supplementary experimental results that complement the main paper. We report the impact of polyline sampling strategies, provide a runtime comparison, analyze the sensitivity of PLD to the cutoff parameter, and include additional qualitative examples.

A.1 Effect of sampling and runtime comparison

Table 4 reports the sensitivity of PLD and its decomposition to the equidistant sampling distance, along with evaluation runtime, benchmarked using StreamMapNet on R_{60} . PLD is stable across sampling distances, with deviations from the 0.5 m baseline below 1%. The localization component $\bar{e}_{loc.}^{(c,p)}$ shows the largest sensitivity, since denser sampling better captures geometric detail, while $\bar{e}_{det.}$ is virtually unaffected. For reference, the sensitivity of PLD is slightly lower than the CD-mAP sensitivity level. In terms of computational cost, at 0.5 m sampling distance, PLD has comparable runtime to CD-mAP, with modest overhead only at finer resolutions. Hence the merits of PLD does not come at the cost of compute time. Since we argue for using PLD with only a single threshold, the current comparison against the standard three-threshold mAP is the relevant practical scenario, where the overhead is negligible. For completeness, Table 4 also includes results for the conventional fixed- N interpolation approach ($N = 200$ points), which matches the mPLD and approximate mAP values of the 0.5 m equidistant baseline but incurs substantially higher runtime, with 238.2 s for PLD and 160.1 s for CD-mAP, compared to 37.8 s and 38.0 s, respectively at 0.5 m equidistant sampling (a factor of approximately 4–6 \times slower). This confirms that equidistant sampling is strictly preferable, as it is not only more intuitive but also yields equivalent metric values while reducing computation time by approximately one order of magnitude.

A.2 Effect of PLD cutoff c

Table 5 shows the effect of the cutoff parameter c on PLD for all baselines on R_{100} . Increasing c from 1.0 to 1.5 to 2.0 consistently reduces overall mPLD for all methods. Looking at the decomposition of error, we see that the reduction is mostly in $\bar{e}_{det.}$, which is expected, since more points are assigned at this threshold. The relative ranking among baselines remains unchanged, confirming the robustness of PLD to this hyperparameter choice.

From another perspective, at $c = 1.0$ the error is very high for all methods on R_{100} , with mPLD values exceeding 0.91. This reflects the current state of OME methods, whose geometric accuracy has not yet reached a level at which a 1.0 m cutoff can meaningfully discriminate between baselines. In contrast, $c = 1.5$ provides a more balanced setting, as it is sufficiently restrictive to penalize genuine localization errors while still allowing enough assignment coverage to reveal informative differences between methods. We therefore adopt $c = 1.5$ in the experiments presented in the main text.

A.3 Additional qualitative examples

Fig. 4 to Fig. 6 provide additional qualitative comparisons between CD-AP and PLD across more scenes, complementing the example shown in the main text. The examples are generated using StreamMapNet on the R_{100} evaluation range. Fig. 4 and Fig. 6 highlight cases where AP assigns a perfect score despite noticeable geometric inaccuracies. Fig. 5 illustrates the failure of AP to correctly capture partial matches, which commonly occurs for dividers. These limitations are effectively

Table 5: Effect of cutoff parameter c on mPLD ($p = 1$) for all baselines on R_{100} .

Baseline	$c = 1.0$			$c = 1.5$			$c = 2.0$		
	↓ mPLD	mLoc.	mDet.	↓ mPLD	mLoc.	mDet.	↓ mPLD	mLoc.	mDet.
Maptrv2	0.955	0.128	0.827	0.936	0.144	0.792	0.921	0.149	0.772
StreamMapNet	0.952	0.158	0.794	0.928	0.188	0.740	0.909	0.197	0.712
MapTracker	0.917	0.221	0.696	0.884	0.227	0.657	0.858	0.217	0.641

addressed by PLD, where both geometric inaccuracies and the fine-grained detection of partial matches lead to more informative scores. Hence, PLD provides a more faithful assessment of OME map quality.

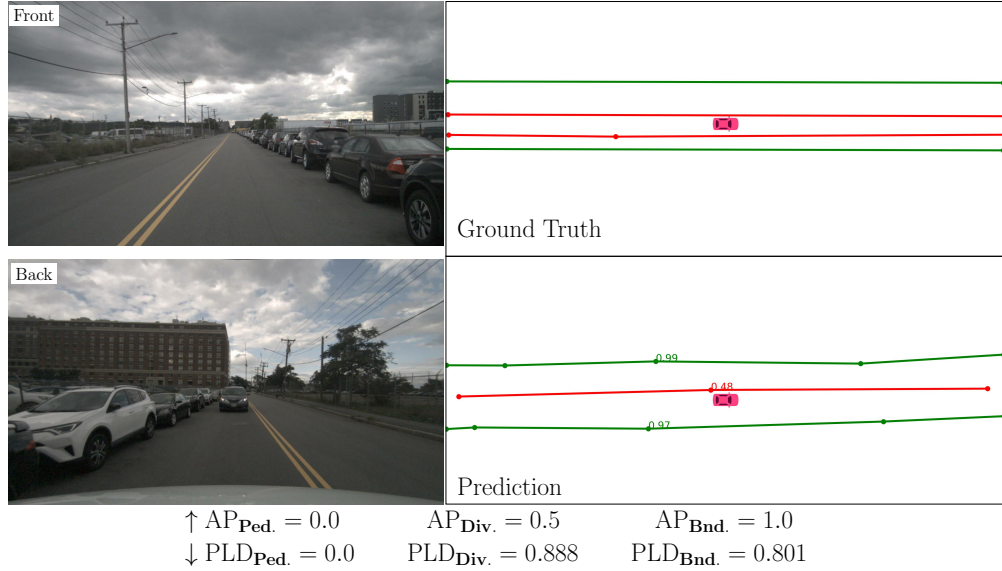


Figure 4: Additional qualitative example from StreamMapNet on R_{100} ($\tau \in \{1.0, 1.5, 2.0\}$ for AP, and $c = 1.5$, $p = 1$ for PLD. Confidences shown on the figure.)

B Proof of the triangle inequality for SOSPA

For an ordered assignment set $\theta \in \Gamma_{|\mathbf{x}|, |\mathbf{y}|}^o$ and finite sequences \mathbf{x} , \mathbf{y} , define the assignment cost

$$C(\theta, \mathbf{x}, \mathbf{y}) = \left(\sum_{(i,j) \in \theta} d(x_i, y_j)^p + \frac{c^p}{2} (|\mathbf{x}| + |\mathbf{y}| - 2|\theta|) \right)^{1/p} \quad (14)$$

so that

$$d_{\text{SOSPA}}^{(c,p)}(\mathbf{x}, \mathbf{y}) = \min_{\theta \in \Gamma_{|\mathbf{x}|, |\mathbf{y}|}^o} C(\theta, \mathbf{x}, \mathbf{y}) \quad (15)$$

B.1 Proof of triangle inequality for non-normalized SOSPA

Theorem 1. *The non-normalized SOSPA defined in (1) satisfies the triangle inequality*

$$d_{\text{SOSPA}}^{(c,p)}(\mathbf{x}, \mathbf{y}) \leq d_{\text{SOSPA}}^{(c,p)}(\mathbf{x}, \mathbf{z}) + d_{\text{SOSPA}}^{(c,p)}(\mathbf{z}, \mathbf{y}) \quad (16)$$

To show Theorem 1, we begin by stating and proving several lemmas.

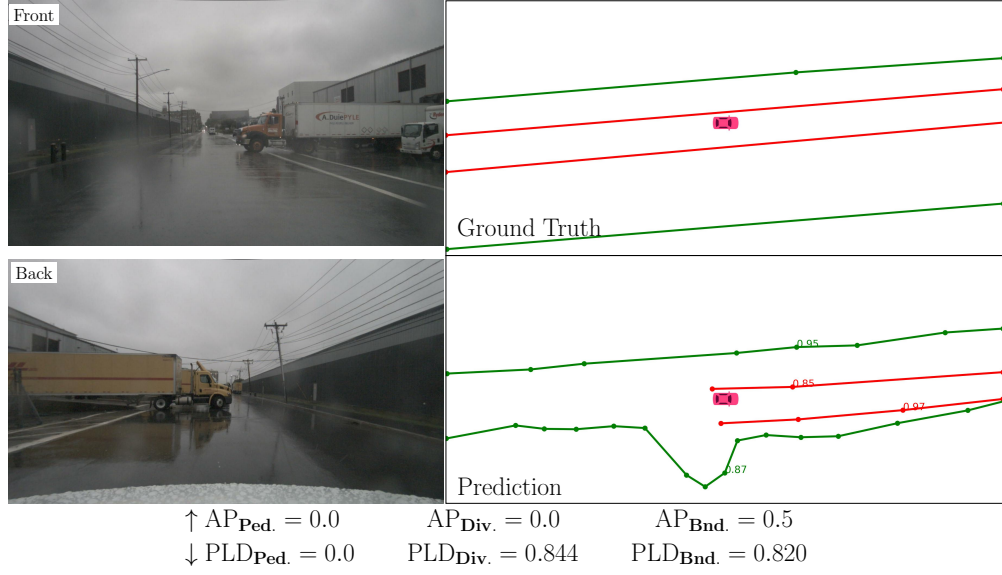


Figure 5: Additional qualitative example from StreamMapNet on R_{100} ($\tau \in \{1.0, 1.5, 2.0\}$ for AP, and $c = 1.5$, $p = 1$ for PLD. Confidences shown on the figure.)

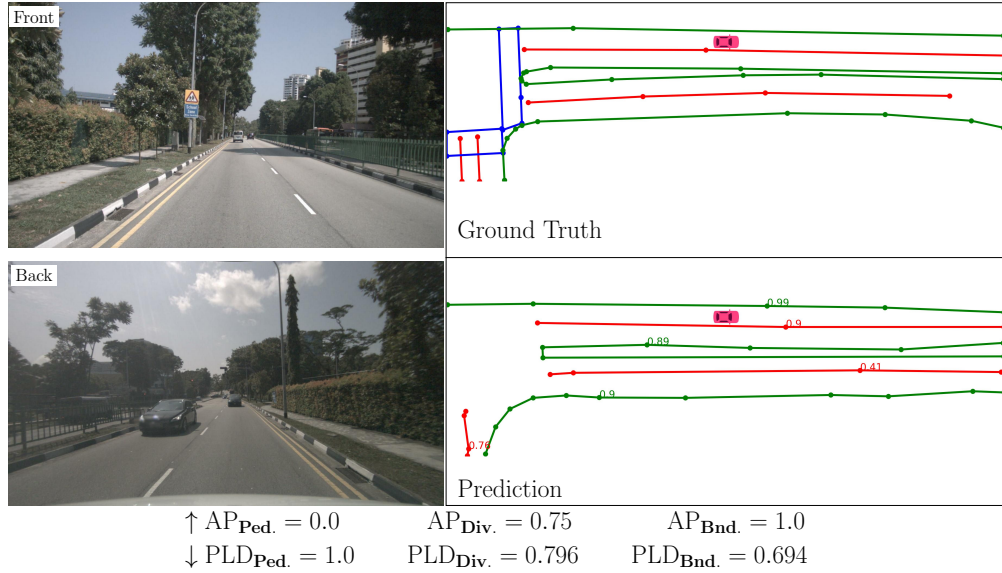


Figure 6: Additional qualitative example from StreamMapNet on R_{100} ($\tau \in \{1.0, 1.5, 2.0\}$ for AP, and $c = 1.5$, $p = 1$ for PLD. Confidences shown on the figure.)

Let $\theta_{x,z} \in \Gamma_{|x|,|z|}^0$ and $\theta_{z,y} \in \Gamma_{|z|,|y|}^0$ be ordered assignment sets. Then we define the composed set θ_c as

$$\theta_c \triangleq \theta_{x,z} \circ \theta_{z,y} = \{(i, m) : (i, j) \in \theta_{x,z} \text{ and } (j, m) \in \theta_{z,y} \text{ for some } j\} \quad (17)$$

Moreover, we define

$$\begin{aligned} J_{x,z} &= \{j : (i, j) \in \theta_{x,z} \text{ for some } i\} \\ J_{z,y} &= \{j : (j, m) \in \theta_{z,y} \text{ for some } m\} \\ J_c &= J_{x,z} \cap J_{z,y} \end{aligned} \quad (18)$$

Observe that $J_{\mathbf{x},\mathbf{z}}$ and $J_{\mathbf{z},\mathbf{y}}$ represents indices in \mathbf{z} matched to \mathbf{x} and \mathbf{y} , respectively.

Lemma 3. *The composed set θ_c defined in (17) is an ordered assignment set between \mathbf{x} and \mathbf{y} , i.e., $\theta_c \in \Gamma_{|\mathbf{x}|,|\mathbf{y}|}^o$.*

Proof. Suppose $(i_1, m_1), (i_2, m_2) \in \theta_c$ with $i_1 < i_2$. By the definition of θ_c , there exist indices j_1, j_2 such that:

$$\begin{aligned} (i_1, j_1) &\in \theta_{\mathbf{x},\mathbf{z}}, & (j_1, m_1) &\in \theta_{\mathbf{z},\mathbf{y}}, \\ (i_2, j_2) &\in \theta_{\mathbf{x},\mathbf{z}}, & (j_2, m_2) &\in \theta_{\mathbf{z},\mathbf{y}}. \end{aligned} \quad (19)$$

Since $\theta_{\mathbf{x},\mathbf{z}} \in \Gamma_{|\mathbf{x}|,|\mathbf{z}|}^o$ is an ordered set and $i_1 < i_2$, the ordering constraint implies $j_1 < j_2$.

Since $\theta_{\mathbf{z},\mathbf{y}} \in \Gamma_{|\mathbf{z}|,|\mathbf{y}|}^o$ is an ordered set and $j_1 < j_2$, the ordering constraint implies $m_1 < m_2$.

Therefore, whenever $i_1 < i_2$ for pairs in θ_c , we have $m_1 < m_2$, which means θ_c satisfies the ordering constraint. Hence, $\theta_c \in \Gamma_{|\mathbf{x}|,|\mathbf{y}|}^o$. \square

Lemma 4. *Let θ_c be as defined in (17) then it follows that*

$$|\theta_{\mathbf{x},\mathbf{z}}| + |\theta_{\mathbf{z},\mathbf{y}}| \leq |\mathbf{z}| + |\theta_c| \quad (20)$$

Proof. Given $J_{\mathbf{x},\mathbf{z}}$, $J_{\mathbf{z},\mathbf{y}}$, and J_c as defined in (18), using the inclusion-exclusion principle we have

$$\begin{aligned} |J_{\mathbf{x},\mathbf{z}} \cup J_{\mathbf{z},\mathbf{y}}| &= |J_{\mathbf{x},\mathbf{z}}| + |J_{\mathbf{z},\mathbf{y}}| - |J_{\mathbf{x},\mathbf{z}} \cap J_{\mathbf{z},\mathbf{y}}| \\ &= |\theta_{\mathbf{x},\mathbf{z}}| + |\theta_{\mathbf{z},\mathbf{y}}| - |\theta_c| \end{aligned} \quad (21)$$

Combining this with the fact that $|J_{\mathbf{x},\mathbf{z}} \cup J_{\mathbf{z},\mathbf{y}}| \leq |\mathbf{z}|$ we establish (20) and the lemma follows. \square

Lemma 5. *Let \mathbf{x} , \mathbf{y} , \mathbf{z} be finite sequences. There exists a valid ordered alignment $\theta_{\mathbf{x},\mathbf{y}} \in \Gamma_{|\mathbf{x}|,|\mathbf{y}|}^o$ such that the alignment cost (14) satisfies*

$$C(\theta_{\mathbf{x},\mathbf{y}}, \mathbf{x}, \mathbf{y}) \leq d_{\text{SOSPA}}^{(c,p)}(\mathbf{x}, \mathbf{z}) + d_{\text{SOSPA}}^{(c,p)}(\mathbf{z}, \mathbf{y}) \quad (22)$$

Proof. Given $J_{\mathbf{x},\mathbf{z}}$, $J_{\mathbf{z},\mathbf{y}}$, and J_c as defined in (18), let $n = |\theta_{\mathbf{x},\mathbf{z}}| + |\theta_{\mathbf{z},\mathbf{y}}| - |\theta_c|$, then let us define two sequences $\mathbf{u}, \mathbf{v} \in \mathbb{R}_{\geq 0}^{n+2}$ as

$$(u_k, v_k) = \begin{cases} (d(x_{\sigma(j)}, z_j), d(z_j, y_{\pi(j)})), & k \leftrightarrow j \in J_c, \\ (d(x_{\sigma(j)}, z_j), 0), & k \leftrightarrow j \in J_{\mathbf{x},\mathbf{z}} \setminus J_c, \\ (0, d(z_l, y_{\pi(l)})), & k \leftrightarrow l \in J_{\mathbf{z},\mathbf{y}} \setminus J_c, \\ (g_{\mathbf{x},\mathbf{z}}^{1/p}, 0) \text{ or } (0, g_{\mathbf{z},\mathbf{y}}^{1/p}), & k = n+1, n+2, \end{cases} \quad (23)$$

where $g_{\mathbf{x},\mathbf{z}} = \frac{c^p}{2}(|\mathbf{x}| + |\mathbf{z}| - 2|\theta_{\mathbf{x},\mathbf{z}}|)$ and $g_{\mathbf{z},\mathbf{y}} = \frac{c^p}{2}(|\mathbf{z}| + |\mathbf{y}| - 2|\theta_{\mathbf{z},\mathbf{y}}|)$, and σ, π are ordered mappings on $\{1, 2, \dots, |\mathbf{x}|\}$, and $\{1, 2, \dots, |\mathbf{y}|\}$, respectively. They satisfy

$$\{(\sigma(j), \pi(j)) : j \in J_c\} = \theta_c \quad (24)$$

By construction, and using (14), we have that

$$C(\theta_{\mathbf{x},\mathbf{z}}, \mathbf{x}, \mathbf{z}) + C(\theta_{\mathbf{z},\mathbf{y}}, \mathbf{z}, \mathbf{y}) = \|\mathbf{u}\|_p + \|\mathbf{v}\|_p \geq \|\mathbf{u} + \mathbf{v}\|_p. \quad (25)$$

where the inequality is obtained by applying, Minkowski's inequality ($1 \leq p$). Expanding the terms, we arrive at

$$\|\mathbf{u} + \mathbf{v}\|_p^p = \sum_{j \in J_c} (d(x_{\sigma(j)}, z_j) + d(z_j, y_{\pi(j)}))^p + \underbrace{A}_{\geq 0} + g_{\mathbf{x},\mathbf{z}} + g_{\mathbf{z},\mathbf{y}} \quad (26)$$

$$\geq \sum_{(i,j) \in \theta_c} d(x_i, y_j)^p + \frac{c^p}{2}(|\mathbf{x}| + |\mathbf{y}| - 2|\theta_c|) + c^p(|\mathbf{z}| + |\theta_c| - |\theta_{\mathbf{x},\mathbf{z}}| - |\theta_{\mathbf{z},\mathbf{y}}|) \quad (27)$$

$$\geq \sum_{(i,j) \in \theta_c} d(x_i, y_j)^p + \frac{c^p}{2}(|\mathbf{x}| + |\mathbf{y}| - 2|\theta_c|) \quad (28)$$

where (27) follows by dropping $A \geq 0$ and applying the triangle inequality on the base metric d . The last inequality holds by applying the result of Lemma 4.

Taking the p -th root in (28), and combining with (25), we obtain

$$C(\theta_c, \mathbf{x}, \mathbf{y}) \leq C(\theta_{\mathbf{x}, \mathbf{z}}, \mathbf{x}, \mathbf{z}) + C(\theta_{\mathbf{z}, \mathbf{y}}, \mathbf{z}, \mathbf{y}) \quad (29)$$

for any valid ordered assignments $\theta_{\mathbf{x}, \mathbf{z}}$ and $\theta_{\mathbf{z}, \mathbf{y}}$. Choosing the optimal assignments, i.e., $C(\theta_{\mathbf{x}, \mathbf{z}}^*, \mathbf{x}, \mathbf{z}) = d_{\text{SOSPA}}^{(c,p)}(\mathbf{x}, \mathbf{z})$ and $C(\theta_{\mathbf{z}, \mathbf{y}}^*, \mathbf{z}, \mathbf{y}) = d_{\text{SOSPA}}^{(c,p)}(\mathbf{z}, \mathbf{y})$, we establish (22), since $\theta_c \in \Gamma_{\mathbf{x}, \mathbf{y}}^0$ is a valid ordered assignment by Lemma 3. \square

Now the result of Theorem 1 follows immediately by the result of Lemma 3 and (15).

B.2 Proof of the triangle inequality for SOSPA normalization

The proof of triangle inequality for $\bar{d}_{\text{SOSPA}}^{(c,p)}$ is similar to that of $\bar{d}_{\text{PLD}}^{(c,p)}$. We therefore demonstrate only the proof for this latter.

C Proof of the triangle inequality for PLD normalization ($p = 1$)

We prove that $\bar{d}_{\text{PLD}}^{(c,p)}$ is a metric for $p = 1$. The proof follows the normalization framework of Li and Liu [17]. We proceed in three steps: (i) we define a PLD similarity measure analogous to the generalized Levenshtein similarity (GLS); (ii) we establish four key properties of this similarity (Theorem 2); and (iii) we use these properties to prove that the normalized distance $\bar{d}_{\text{PLD}}^{(c,p)}$ satisfies the triangle inequality and is therefore a metric (Theorem 3).

Definition 5 (PLD Similarity). For $p = 1$, we define PLD similarity between two sets of polylines \mathbf{X} and \mathbf{Y} is

$$S_{\text{PLD}}^{(c,p)}(\mathbf{X}, \mathbf{Y}) = \frac{\frac{1}{2}(R_{\mathbf{X}} + R_{\mathbf{Y}}) - d_{\text{PLD}}^{(c,p)}(\mathbf{X}, \mathbf{Y})}{2}. \quad (30)$$

Theorem 2 (GLS properties for DAP). Let $p = 1$. For any three sets of polylines $\mathbf{X}, \mathbf{Y}, \mathbf{Z}$, the GLS from Definition 5 satisfies:

- (i) $S_{\text{PLD}}^{(c,p)}(\mathbf{X}, \mathbf{X}) = \frac{1}{2} R_{\mathbf{X}}$,
- (ii) $S_{\text{PLD}}^{(c,p)}(\mathbf{X}, \mathbf{Y}) = S_{\text{PLD}}^{(c,p)}(\mathbf{Y}, \mathbf{X})$,
- (iii) $0 \leq S_{\text{PLD}}^{(c,p)}(\mathbf{X}, \mathbf{Y}) \leq \min\{S_{\text{PLD}}^{(c,p)}(\mathbf{X}, \mathbf{X}), S_{\text{PLD}}^{(c,p)}(\mathbf{Y}, \mathbf{Y})\} = \frac{1}{2} \min\{R_{\mathbf{X}}, R_{\mathbf{Y}}\}$,
- (iv) $S_{\text{PLD}}^{(c,p)}(\mathbf{Y}, \mathbf{Y}) + S_{\text{PLD}}^{(c,p)}(\mathbf{X}, \mathbf{Z}) \geq S_{\text{PLD}}^{(c,p)}(\mathbf{X}, \mathbf{Y}) + S_{\text{PLD}}^{(c,p)}(\mathbf{Y}, \mathbf{Z})$.

These are the direct analogues of properties (1)–(4) in Theorem 1 of [17], with $\lambda = 1/2$ and $|\cdot|$ replaced by $R_{(\cdot)}$.

Proof. Before we show the properties we first establish few basic results.

Lemma 6. For $p \geq 1$, the PLD metric satisfies:

$$d_{\text{PLD}}^{(c,p)}(\mathbf{X}, \mathbf{Y}) \leq \left(\frac{1}{2}(R_{\mathbf{X}} + R_{\mathbf{Y}}) \right)^{1/p} \quad (31)$$

Proof. The bound is obtained by using the empty assignment $\theta = \emptyset$ in Definition 4. With no matched pairs, all elements are unassigned, and the bound (31) follows. \square

Lemma 7. For $p \geq 1$, the PLD metric satisfies:

$$d_{\text{PLD}}^{(c,p)}(\mathbf{X}, \mathbf{Y}) \geq \left(\frac{1}{2} |R_{\mathbf{X}} - R_{\mathbf{Y}}| \right)^{1/p} \quad (32)$$

Proof. Recall Definition 4. Since $\bar{d}_{\text{SOSPA}}^{(c,p)}(\mathbf{x}_i, \mathbf{y}_j) \geq 0$ and $\min(r_{\mathbf{x}_i}, r_{\mathbf{y}_j}) \geq 0$, we can lower bound by ignoring the non-negative localization terms

$$d_{\text{PLD}}^{(c,p)}(\mathbf{X}, \mathbf{Y})^p \geq \frac{1}{2} \min_{\theta \in \Gamma} \left(\sum_{(i,j) \in \theta} |r_{\mathbf{x}_i} - r_{\mathbf{y}_j}| + \sum_{i: \forall j, (i,j) \notin \theta} r_{\mathbf{x}_i} + \sum_{j: \forall i, (i,j) \notin \theta} r_{\mathbf{y}_j} \right) \quad (33)$$

Recalling $R_{\mathbf{X}} = \sum_i r_{\mathbf{x}_i}$ and $R_{\mathbf{Y}} = \sum_j r_{\mathbf{y}_j}$. Using the identity $|r_{\mathbf{x}_i} - r_{\mathbf{y}_j}| = r_{\mathbf{x}_i} + r_{\mathbf{y}_j} - 2 \min(r_{\mathbf{x}_i}, r_{\mathbf{y}_j})$, (33) simplifies to

$$d_{\text{PLD}}^{(c,p)}(\mathbf{X}, \mathbf{Y})^p \geq \frac{1}{2} \min_{\theta \in \Gamma} \left(R_{\mathbf{X}} + R_{\mathbf{Y}} - 2 \sum_{(i,j) \in \theta} \min(r_{\mathbf{x}_i}, r_{\mathbf{y}_j}) \right)$$

The term $\sum_{(i,j) \in \theta} \min(r_{\mathbf{x}_i}, r_{\mathbf{y}_j})$ is maximized when we match elements optimally, but we can only match up to $\min(R_{\mathbf{X}}, R_{\mathbf{Y}})$ total probability. Therefore,

$$\begin{aligned} d_{\text{PLD}}^{(c,p)}(\mathbf{X}, \mathbf{Y})^p &\geq \frac{1}{2} (R_{\mathbf{X}} + R_{\mathbf{Y}} - 2 \min(R_{\mathbf{X}}, R_{\mathbf{Y}})) \\ &= \frac{1}{2} |R_{\mathbf{X}} - R_{\mathbf{Y}}| \end{aligned} \quad (34)$$

Taking the p -th root of both sides yields (32). \square

Now we can readily show the properties of PLD similarity.

Property (i). Follows directly from $d_{\text{PLD}}^{(c,p)}(\mathbf{X}, \mathbf{X}) = 0$.

Property (ii). Follows from $d_{\text{PLD}}^{(c,p)}(\mathbf{X}, \mathbf{Y}) = d_{\text{PLD}}^{(c,p)}(\mathbf{Y}, \mathbf{X})$.

Property (iii). *Lower bound.* From Lemma 6, it follows that $S_{\text{PLD}}^{(c,p)}(\mathbf{X}, \mathbf{Y}) \geq 0$.

Upper bound. By Lemma 7 with $p = 1$, $d_{\text{PLD}}^{(c,p)}(\mathbf{X}, \mathbf{Y}) \geq \frac{1}{2} |R_{\mathbf{X}} - R_{\mathbf{Y}}|$. Substituting:

$$\begin{aligned} S_{\text{PLD}}^{(c,p)}(\mathbf{X}, \mathbf{Y}) &\leq \frac{\frac{1}{2}(R_{\mathbf{X}} + R_{\mathbf{Y}}) - \frac{1}{2}|R_{\mathbf{X}} - R_{\mathbf{Y}}|}{2} \\ &= \frac{1}{2} \min\{R_{\mathbf{X}}, R_{\mathbf{Y}}\}. \end{aligned} \quad (35)$$

By property (i), we obtain $S_{\text{PLD}}^{(c,p)}(\mathbf{X}, \mathbf{Y}) \leq \min\{S_{\text{PLD}}^{(c,p)}(\mathbf{X}, \mathbf{X}), S_{\text{PLD}}^{(c,p)}(\mathbf{Y}, \mathbf{Y})\}$.

Property (iv). By the triangle inequality for $d_{\text{PLD}}^{(c,p)}$

$$d_{\text{PLD}}^{(c,p)}(\mathbf{X}, \mathbf{Y}) + d_{\text{PLD}}^{(c,p)}(\mathbf{Y}, \mathbf{Z}) \geq d_{\text{PLD}}^{(c,p)}(\mathbf{X}, \mathbf{Z}). \quad (36)$$

Expanding using (30) and reshuffling, we reach

$$\frac{1}{2} R_{\mathbf{Y}} + S_{\text{PLD}}^{(c,p)}(\mathbf{X}, \mathbf{Z}) \geq S_{\text{PLD}}^{(c,p)}(\mathbf{X}, \mathbf{Y}) + S_{\text{PLD}}^{(c,p)}(\mathbf{Y}, \mathbf{Z}) \quad (37)$$

Substituting $S_{\text{PLD}}^{(c,p)}(\mathbf{Y}, \mathbf{Y}) = \frac{1}{2} R_{\mathbf{Y}}$ (from property (i)), yields property (iv). \square

Theorem 3 (Normalized PLD is a metric). *Let $p = 1$. The normalized PLD*

$$\bar{d}_{\text{PLD}}^{(c,p)}(\mathbf{X}, \mathbf{Y}) = \frac{2 d_{\text{PLD}}^{(c,p)}(\mathbf{X}, \mathbf{Y})}{\frac{1}{2}(R_{\mathbf{X}} + R_{\mathbf{Y}}) + d_{\text{PLD}}^{(c,p)}(\mathbf{X}, \mathbf{Y})} \quad (38)$$

is a metric valued in $[0, 1]$.

Proof. Identity and symmetry follow directly from the corresponding properties of $d_{\text{PLD}}^{(c,p)}$. As for the triangle inequality, the proof follows the same argument as in [17, Theorem 2]. The four properties established in Theorem 2 mirror the result in [17, Theorem 1], where for string edit distance with

uniform deletion/insertion cost λ , the GLS is defined as $\text{GLS}(X, Y) = \frac{\lambda(|X|+|Y|)-d(X,Y)}{2}$. In our setting, $\lambda = 1/2$, and $R_{\mathbf{x}}, R_{\mathbf{y}}$ play the role of the string lengths $|X|$ and Y , respectively.

Note that $d_{\text{PLD}}^{(c,p)}$ is itself a metric for $p = 1$, and its base single-instance metric $\bar{d}_{\text{SOSPA}}^{(c,p)}$ (Definition 2) is a metric as established in the main document. This ensures all prerequisites are met for the argument in [17, Theorem 2] to hold. \square

D Proof of Lemma 2

To show the lemma, we first establish the following result.

Lemma 8. *Let $\theta \in \Gamma_{|\mathbf{x}|, |\mathbf{y}|}^o$ be an ordered assignment set for $(\mathbf{x}, \mathcal{S}_{s_y}(\mathbf{y}))$ for some $s_y \in \{0, \dots, |\mathbf{y}| - 1\}$. Then there exist an ordered assignment set $\bar{\theta} \in \Gamma_{|\mathbf{x}|, |\mathbf{y}|}^o$ and an integer $l \in \{0, \dots, |\mathbf{y}| - 1\}$, such that*

$$C(\theta, \mathbf{x}, \mathcal{S}_{s_y}(\mathbf{y})) = C(\bar{\theta}, \mathcal{S}_1(\mathbf{x}), \mathcal{S}_l(\mathbf{y})), \quad (39)$$

where C is defined in (14).

Proof. Let $\mathbf{y}' = \mathcal{S}_{s_y}(\mathbf{y})$ for some s_y . Let $\pi_1(\theta) = \{(i, j) \in \theta\}$. To show (39), we identify two cases. The case $1 \in \pi_1(\theta)$, and the case $1 \notin \pi_1(\theta)$

Case 1: Let $(1, j_0) \in \theta$ for some j_0 . We can partition the assignment set following

$$\theta = \{(1, j_0)\} \cup \theta_R^*, \quad \text{where } \theta_R^* \subseteq \{2, \dots, |\mathbf{x}|\} \times \{j_0 + 1, \dots, |\mathbf{y}|\}. \quad (40)$$

Following this, and recalling the definition of the operator $\langle k \rangle$ (5), we define $\bar{\theta}$ as

$$\begin{aligned} \bar{\theta} &= \{(i-1, j-j_0) : (i, j) \in \theta_R^*\} \cup \{(|\mathbf{x}|, |\mathbf{y}|\}) \\ &= \{(\langle i-1 \rangle_{|\mathbf{x}|}, \langle j-j_0 \rangle_{|\mathbf{y}|}) : (i, j) \in \theta\} \end{aligned} \quad (41)$$

Observing (40) and the fact that $(\langle i-1 \rangle_{|\mathbf{x}|}, \langle j-j_0 \rangle_{|\mathbf{y}|}) = (|\mathbf{x}|, |\mathbf{y}|)$ for the pair $(1, j_0)$, it is easy to establish that $\bar{\theta} \in \Gamma_{|\mathbf{x}|, |\mathbf{y}|}^o$ with $|\bar{\theta}| = |\theta|$.

Let $l = \langle s_y + j_0 \rangle_{|\mathbf{y}|}$ and let $\mathbf{y}'' = \mathcal{S}_{j_0}(\mathbf{y}') = \mathcal{S}_l(\mathbf{y})$. We use $\bar{\theta}$ as an assignment set between $\mathbf{x}' = \mathcal{S}_1(\mathbf{x})$ and \mathbf{y}'' . Then,

$$\begin{aligned} \sum_{(i', j') \in \bar{\theta}} d(x'_{i'}, y''_{j'})^p &= \sum_{(i', j') \in \bar{\theta}} d(x_{\langle i'+1 \rangle_{|\mathbf{x}|}}, y'_{\langle j'+j_0 \rangle_{|\mathbf{y}|}})^p \\ &= \sum_{(i, j) \in \theta} d(x_i, y'_j)^p \end{aligned} \quad (42)$$

since

$$\begin{aligned} \langle j' + j_0 \rangle_{|\mathbf{y}|} &= \langle \langle j - j_0 \rangle_{|\mathbf{y}|} + j_0 \rangle_{|\mathbf{y}|} \\ &= \langle (j - j_0 - 1) \bmod |\mathbf{y}| + 1 + j_0 \rangle_{|\mathbf{y}|} \\ &= \langle (j - j_0 - 1) \bmod |\mathbf{y}| + j_0 \rangle_{|\mathbf{y}|} \bmod |\mathbf{y}| + 1 \\ &= j \end{aligned} \quad (43)$$

and similarly, $\langle i' + 1 \rangle_{|\mathbf{x}|} = \langle \langle i - 1 \rangle_{|\mathbf{x}|} + 1 \rangle_{|\mathbf{x}|} = i$. Given the result above, recalling (14), and using the fact that $|\bar{\theta}| = |\theta|$ we can easily arrive at

$$C(\theta, \mathbf{x}, \mathcal{S}_{s_y}(\mathbf{y})) = C(\bar{\theta}, \mathcal{S}_1(\mathbf{x}), \mathcal{S}_l(\mathbf{y})) \quad (44)$$

where $l = \langle s_y + j_0 \rangle_{|\mathbf{y}|}$ and hence (39) holds for the case $(1, j_0) \in \theta$ for some $1 \leq j_0 \leq |\mathbf{y}|$.

Case 2: The proof for the case $1 \notin \pi_1(\theta)$, can be addressed by defining a mapping $\bar{\theta} = \{(i-1, j) : (i, j) \in \theta\}$ and following similar steps as done earlier, to show that $C(\theta, \mathbf{x}, \mathcal{S}_{s_y}(\mathbf{y})) = C(\bar{\theta}, \mathcal{S}_1(\mathbf{x}), \mathcal{S}_l(\mathbf{y}))$, where $l = s_y$. \square

Proof of Lemma 2. We want to show that

$$d_{\text{SOSPA}}^{(c,p)}([\mathbf{x}], [\mathbf{y}]) = d_{\text{SOSPA}}^{(c,p)}(\mathbf{x}, [\mathbf{y}]) \quad (45)$$

To that end, define

$$f(s_x) \triangleq \min_{s_y \in \{0, 1, \dots, |\mathbf{y}|-1\}} d_{\text{SOSPA}}^{(c,p)}(\mathcal{S}_{s_x}(\mathbf{x}), \mathcal{S}_{s_y}(\mathbf{y})) \quad (46)$$

so that $d_{\text{SOSPA}}^{(c,p)}([\mathbf{x}], [\mathbf{y}]) = \min_{s_x} f(s_x)$. To prove (8), it is enough to show that $f(s_x)$ is independent of s_x , i.e., $f(s_x) = f(0)$ for all $s_x \in \{0, \dots, |\mathbf{x}|-1\}$. We follow a similar argument to the one outlined in [12, Lemma 3.1].

Observe that it suffices to show $f(1) \leq f(0)$. Since the same argument applied iteratively yields

$$f(0) \geq f(1) \geq \dots \geq f(|\mathbf{x}|) = f(0) \quad (47)$$

forcing equality.

Now, Let s_y^* achieve the minimum in $f(0)$ and let $\theta^* \in \Gamma_{|\mathbf{x}|, |\mathbf{y}|}^0$ be the optimal assignment for $(\mathbf{x}, \mathcal{S}_{s_y^*}(\mathbf{y}))$, so that $f(0) = C(\theta^*, \mathbf{x}, \mathcal{S}_{s_y^*}(\mathbf{y}))$.

By Lemma 8, there exist $\bar{\theta} \in \Gamma_{|\mathbf{x}|, |\mathbf{y}|}^0$ and $l \in \{0, \dots, |\mathbf{y}|-1\}$ such that

$$C(\theta^*, \mathbf{x}, \mathcal{S}_{s_y^*}(\mathbf{y})) = C(\bar{\theta}, \mathcal{S}_1(\mathbf{x}), \mathcal{S}_l(\mathbf{y})). \quad (48)$$

Therefore,

$$\begin{aligned} f(1) &\leq d_{\text{SOSPA}}^{(c,p)}(\mathcal{S}_1(\mathbf{x}), \mathcal{S}_l(\mathbf{y})) \\ &\leq C(\bar{\theta}, \mathcal{S}_1(\mathbf{x}), \mathcal{S}_l(\mathbf{y})) = f(0). \end{aligned} \quad (49)$$

By (47), $f(s_x) = f(0)$ for all s_x , yielding (8). \square